

Fast holonomic quantum computation on superconducting circuits with optimal control

Sai Li, Tao Chen, and Zheng-Yuan Xue*

arXiv:1905.11263v3 [quant-ph] 27 Jan 2020

Geometric phases induced in quantum evolutions have built-in noise-resilient characters, and thus can find applications in many robust quantum manipulation tasks. Here, we propose a feasible and fast scheme for universal quantum computation on superconducting circuits with nonadiabatic non-Abelian geometric phases, using resonant interaction of three-level quantum system. In our scheme, arbitrary single-qubit quantum gates can be implemented in a single-loop scenario by shaping both the amplitudes and phases of the two driving microwave fields resonantly coupled to a transmon device. Moreover, nontrivial two-qubit gates can also be realized with an auxiliary transmon simultaneously coupled to the two target transmons in an effective resonant way. In particular, our proposal can be compatible to various optimal control techniques, which further enhances the robustness of the quantum operations. Therefore, our proposal represents a promising way towards fault-tolerant quantum computation on solid-state quantum circuits.

1 Introduction

High-fidelity quantum gates are essential for the physical realization of quantum computation (QC), and thus constructing noise-resistant gate is one of the key ingredients. Meanwhile, geometric phases [1–3], determined by the global properties of the evolution paths, possess a kind of built-in noise-resilience feature against certain types of local noises [4–7]. Therefore, in large scale quantum systems, where control lines/devices will inevitably cause local noises, it is more promising to realize quantum manipulations in a geometric strategy [8]. Furthermore, the non-Abelian geometric phases [2] can naturally be used to construct universal set of single-qubit gates, and together with a nontrivial two-qubit entangling gate, holonomic QC [9] can be achieved.

Due to the limited coherent times of quantum systems [10, 11], the physical realization of holonomic QC based on fast nonadiabatic evolution, i.e., the nonadiabatic holonomic QC (NHQC) [12, 13], is highly desirable. Recently, the NHQC have achieved significant theoretical [14–33] and experimental progress [34–46]. Among these schemes, due to the easy integrability and flexibility, superconducting circuits system [47–51] is recognized as a promising candidate to implement scalable QC. However, up to now, a practical implementation of NHQC on superconducting circuits is lacking, e.g., experimental demonstrations [34, 41, 45] are limited to the single-qubit gates cases and the more difficult two-qubit gate do not have a feasible scheme yet, due to the need of a nonlinear quantum bus for the two target qubits [29, 44]. Meanwhile, this type of NHQC implementation is sensitive to the systematic error [52–54], which thus smear the main advantage of quantum computation with geometric phases.

Here, to remove the two main obstacles, we propose a practical and fast scheme to construct universal holonomic quantum gates for NHQC on superconducting circuits, by generalizing the previous used single time-dependent variable of Hamiltonian into a two time-dependent variables case. In our scheme, each transmon device serves as a qubit and we only use resonant sequential transitions, driven by two microwave fields, of the ladder type three levels in a transmon device. Meanwhile, the evolution state is set by inverse engineering of the system Hamiltonian, and thus during the cyclic evolution, it can always fulfill the time-dependent Schrödinger equation of the govern Hamiltonian, i.e., no nonadiabatic transitions will occur [55]. In addition, at the end of the

* Corresponding author. E-mail: zyxue83@163.com

S. Li, T. Chen, Prof. Z.-Y. Xue
Guangdong Provincial Key Laboratory of Quantum Engineering and Quantum Materials,
GPETR Center for Quantum Precision Measurement,
School of Physics and Telecommunication Engineering,
South China Normal University,
Guangzhou 510006, China

evolution, the pure geometric phase can be acquired after canceling the dynamical phase, thus the proposed gates are of the geometric nature. In this way, arbitrary single-qubit quantum gates can be implemented in a single-loop scenario by shaping both the amplitudes and phases of two microwave fields. Moreover, without introducing a quantum bus, nontrivial two-qubit gates can be realized with an auxiliary transmon simultaneously coupled to the two target transmons in an effective resonant way and the intrinsic nonlinearity of the auxiliary transmon is large enough for our purpose. In particular, due to the inverse Hamiltonian engineering, the evolution state of our proposal has two independent variables, thus it can be compatible to various optimal control techniques [55, 56] and further enhances the robustness of the quantum operations.

2 Universal single-qubit gates

We now proceed to present our scheme based on superconducting circuits via inverse engineering Hamiltonian by solving the Schrödinger equation [55]. Firstly, arbitrary single-qubit gates can be implemented by using two resonant driving microwave fields with time dependent amplitudes and phases. Then, we show that our scheme is compatible with optimal control methods, thus the robustness of our implementation can be further improved.

2.1 Inverse engineering of Hamiltonian

In this section, we introduce how to inversely engineer the Hamiltonian based on the Schrödinger equation [55] on superconducting circuits. In a superconducting transmon device, we consider the three lowest levels $|g\rangle$, $|e\rangle$ and $|f\rangle$, with $|g\rangle$, $|f\rangle$ being our qubit states and $|e\rangle$ being an auxiliary state, to construct geometric manipulation of the device. As shown in Fig. 1(a), two microwave fields $\Omega_j(t) \cos(\omega_j t + \phi_j(t))$ ($j = 1, 2$), with $\Omega_j(t)$, ω_j and $\phi_j(t)$ being the amplitudes, frequencies and phases, resonantly coupled to the sequential transitions of the three lowest levels of a transmon [29]. Ignoring the higher order oscillating terms, assuming $\hbar = 1$ hereafter, the effective interaction Hamiltonian can be written as

$$H_1 = \left[\frac{\Omega_1(t)}{2} e^{i\phi_1(t)} |g\rangle\langle e| + \frac{\Omega_2(t)}{\sqrt{2}} e^{-i\phi_2(t)} |f\rangle\langle e| \right] |e\rangle\langle e| + \text{H.c.} \\ = \Omega e^{i\phi_1(t)} |b\rangle\langle e| + \text{H.c.}, \quad (1)$$

where $\Omega = \sqrt{(\frac{\Omega_1(t)}{2})^2 + (\frac{\Omega_2(t)}{\sqrt{2}})^2}$, bright state $|b\rangle = \sin(\theta/2)|g\rangle - \cos(\theta/2)e^{-i\phi}|f\rangle$ with $\tan(\theta/2) = \frac{\Omega_1}{\sqrt{2}\Omega_2}$ and $\phi = \phi_2(t) +$

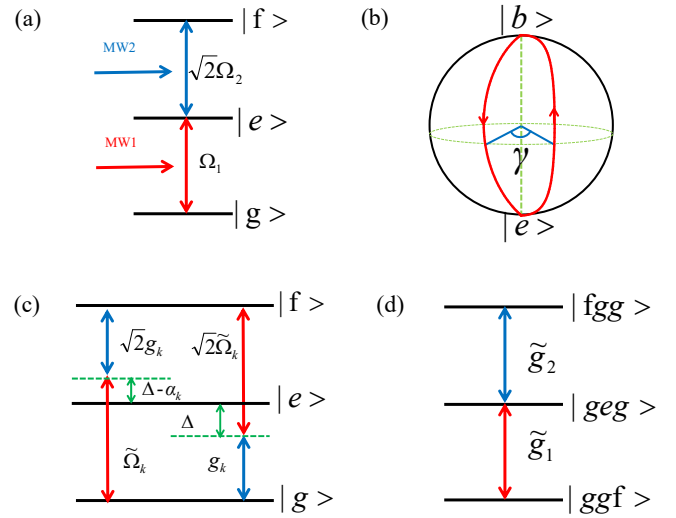


Figure 1 Illustration of the proposal. (a) The three-level configuration of the resonant situation for the single-qubit gates, with two microwave fields resonantly coupled to the three levels of a transmon device. (b) Geometric diagram of the proposed single-qubit gate. (c) Effective resonant qubit-qubit coupling configuration induced by two driving qubits coupled to an auxiliary transmon for non-trivial two qubit gates. (d) The effective coupling configuration for two-qubit gate in the single-excitation subspace.

$\phi_1(t) + \pi$ being time independent, and dark state $|d\rangle = -\cos(\theta/2)e^{i\phi}|g\rangle - \sin(\theta/2)|f\rangle$ is decoupled.

The Hamiltonian H_1 satisfies the Schrödinger equation of

$$i \frac{\partial}{\partial t} |\Psi(t)\rangle = H_1(t) |\Psi(t)\rangle, \quad (2)$$

where the evolution state $|\Psi(t)\rangle$ can generally be parameterized in the $\{|b\rangle, |e\rangle\}$ subspace by using two angles χ, φ and with a global phase f as

$$|\Psi(t)\rangle = e^{-if/2} \begin{pmatrix} \cos \frac{\chi}{2} e^{-i\varphi/2} \\ \sin \frac{\chi}{2} e^{i\varphi/2} \end{pmatrix}. \quad (3)$$

Inserting $|\Psi(t)\rangle$ into the Schrödinger equation, we get

$$\dot{f} = -\dot{\varphi} \cos \chi, \quad \dot{\chi} = -2\Omega \sin(\phi_1 + \varphi), \\ \dot{\varphi} = -2\Omega \cot \chi \cos(\phi_1 + \varphi). \quad (4)$$

That is to say, if the parameters of the two microwave fields satisfy the above relations, the evolution path will just go along with the evolution state $|\Psi(t)\rangle$, i.e., no transitions from the state $|\Psi(t)\rangle$ to its orthogonal states will occur during the quantum evolution governed by Hamiltonian $H_1(t)$ [55].

2.2 Gates implementation and performance

Now, we proceed to implement arbitrary holonomic single-qubit gates. A set of proper parameters χ and φ can be chosen to realize a certain evolution, and once the parameters χ and φ are set, the corresponding Ω and ϕ_1 can be obtained by solving the Eq. (4), i.e.,

$$\phi_1 = \arctan\left(\frac{\dot{\chi}}{\dot{\varphi}} \cot \chi\right) - \varphi, \quad \Omega = -\frac{\dot{\chi}}{2 \sin(\phi_1 + \varphi)}, \quad (5)$$

and thus fix the Hamiltonian $H_1(t)$. Here, we consider a cyclic evolution, which can be achieved by setting $\chi(0) = \chi(\tau) = 0$ in Eq. (3), i.e., the state will start from $|b\rangle$ state and go back to it after an periodical evolution with time τ , only acquiring a phase factor. During the process, the phase factor may consist of both the geometric and the dynamical ones, and the dynamical phase is calculated to be

$$\gamma_d(\tau) = -\int_0^\tau \langle \Psi(t) | H_1 | \Psi(t) \rangle dt = \int_0^\tau \frac{\dot{\varphi} \sin^2 \chi}{2 \cos \chi} dt. \quad (6)$$

In order to induce a pure geometric phase, the dynamical phase should be zero at the end of the cyclic evolution, i.e., $\gamma_d(\tau) = 0$, which is mainly different than the previous NHQC schemes, for instance, $\gamma_d(t) = 0$ should be fulfilled at any moment. However, under this strict condition, there is just one adjustable variable in the Hamiltonian which results in the previous NHQC schemes being sensitive to the systematic error [52–54]. Here, our scheme make the difference in order to release the strict condition to acquire one more adjustable variable to realize more robust quantum evolution process.

In the following, we adopt a single-loop evolution path [22, 29], as illustrated in Fig. 1(b), to induce a pure geometric phase that can be used to achieve universal single-qubit gates. Specifically, the evolution path is divided into two equal parts, in the first path $t \in [0, \tau/2]$, we set

$$\chi_1 = \pi \sin^2\left(\frac{\pi t}{\tau}\right), \quad \varphi_1 = -\frac{\pi}{5} \sin\left(\frac{2\pi t}{\tau}\right) - \frac{\pi}{2}, \quad (7)$$

the corresponding evolution operator is $U_1 = |d\rangle\langle d| + e^{i\gamma_1}|e\rangle\langle b| + e^{-i\gamma_1}|b\rangle\langle e|$. In the second path $t \in [\tau/2, \tau]$, we choose

$$\chi_2 = \pi \sin^2\left(\frac{\pi t}{\tau}\right), \quad \varphi_2 = \frac{\pi}{5} \sin\left(\frac{2\pi t}{\tau}\right) - \gamma - \frac{\pi}{2}, \quad (8)$$

where γ is an arbitrary constant angle. The corresponding evolution operator is $U_2 = |d\rangle\langle d| + e^{i\gamma_2}|b\rangle\langle e| + e^{-i\gamma_2}|e\rangle\langle b|$. Then, the final evolution operator can be obtained as

$$U(\tau) = U_2 U_1 = |d\rangle\langle d| + e^{i\gamma}|b\rangle\langle b| = e^{i\frac{\gamma}{2}} e^{-i\frac{\gamma}{2} \mathbf{n} \cdot \boldsymbol{\sigma}} \quad (9)$$

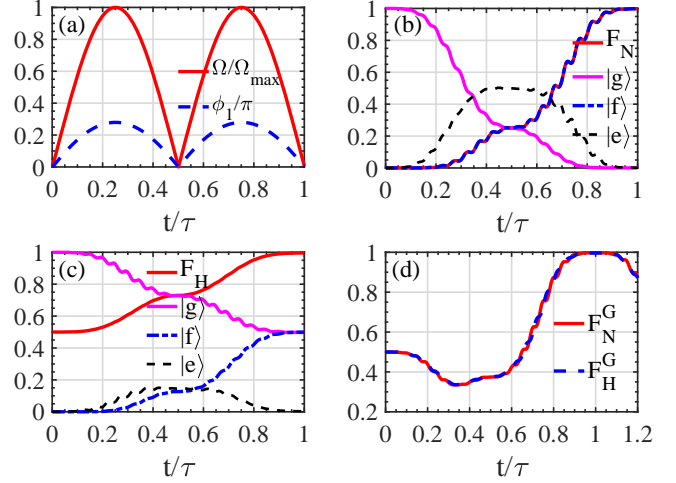


Figure 2 Engineering the single-qubit gates and their performance. (a) The parameter shapes of the Hamiltonian $H_1(t)$. (b) and (c) describe the state population and fidelity dynamics of the NOT gate and the Hadamard gate, respectively. (d) The gate fidelity dynamics of NOT gate and Hadamard gate.

where $\gamma = \gamma_1 + \gamma_2$, $\mathbf{n} = (\sin \theta \cos \phi, -\sin \theta \sin \phi, \cos \theta)$, σ are Pauli matrices. The evolution operator is a rotation operator around the axis \mathbf{n} by an angle γ , can be used to generate arbitrary single-qubit gates in a holonomic way. Especially, we note that when $\dot{\varphi}$ or $\dot{\chi}$ is zero, i.e., $\chi = \pi \sin^2(\pi t/\tau)$ but $\varphi_{1,2}$ are constant, our scheme reduce to the previous NHQC one.

The performance of the single-qubit gate can be evaluated by the Lindblad master equation of

$$\dot{\rho}_1 = i[\rho_1, H_1] + \frac{1}{2} [\Gamma_1 \mathcal{L}(\sigma_1) + \Gamma_2 \mathcal{L}(\sigma_2)], \quad (10)$$

where ρ_1 is the density matrix of the considered system and $\mathcal{L}(\mathcal{A}) = 2\mathcal{A}\rho_1\mathcal{A}^\dagger - \mathcal{A}^\dagger\mathcal{A}\rho_1 - \rho_1\mathcal{A}^\dagger\mathcal{A}$ is the Lindbladian of the operator \mathcal{A} , $\sigma_1 = |g\rangle\langle e| + \sqrt{2}|e\rangle\langle f| + \sqrt{3}|f\rangle\langle h|$, $\sigma_2 = |e\rangle\langle e| + 2|f\rangle\langle f| + 3|h\rangle\langle h|$ with $|h\rangle$ being the third excited state of a transmon, Γ_1 and Γ_2 are the corresponding decay and dephasing rates. Here, we consider the case $\Gamma_1 = \Gamma_2 = \Gamma = 2\pi \times 5$ kHz [57], corresponding to a coherent time of $32 \mu\text{s}$, which is well accessible with current technologies. The anharmonicity of the transmon is set to be $\alpha = \omega_{ge} - \omega_{ef} = 2\pi \times 400$ MHz [58]. Assuming the initial state $|\psi_1\rangle = |g\rangle$ and $\tau \approx 51$ ns, the shapes of Ω and ϕ_1 are shown in Fig. 2(a) with $\Omega_{max} = 2\pi \times 16$ MHz. Note that there will be a bounded maximum amplitude due to the limited anharmonicity of the transmon device. Then, the NOT gate with $\theta = \pi/2$, $\phi = 0$, $\gamma = \pi$ and the Hadamard gate with $\theta = \pi/4$, $\phi = 0$, $\gamma = \pi$ are evaluated, using the

state fidelity defined by $F_{N/H} = {}_{N/H} \langle \psi_f | \rho_1 | \psi_f \rangle_{N/H}$ with $|\psi_f\rangle_N = |f\rangle$ and $|\psi_f\rangle_H = (|g\rangle + |f\rangle)/\sqrt{2}$ being the corresponding target state. The obtained fidelities are as high as $F_N = 99.79\%$ and $F_H = 99.55\%$, as shown in Fig. 2(b) and Fig. 2(c), respectively. The infidelity is mainly due to both the leakage caused by the small anharmonicity and relaxation and dephasing of the qubits and auxiliary state $|e\rangle$. In addition, for a general initial state $|\psi_1\rangle = \cos\theta'|g\rangle + \sin\theta'|f\rangle$, the NOT and Hadamard gates should result in an ideal final state $|\psi_f\rangle_N = \sin\theta'|g\rangle + \cos\theta'|f\rangle$ and $|\psi_f\rangle_H = \frac{1}{\sqrt{2}}[(\cos\theta' + \sin\theta')|g\rangle + (\cos\theta' - \sin\theta')|f\rangle]$. To fully evaluate the performance of the implemented gates, we define the gate fidelity as $F_{N/H}^G = (\frac{1}{2\pi}) \int_0^{2\pi} {}_{N/H} \langle \psi_f | \rho_1 | \psi_f \rangle_{N/H} d\theta'$ [59] with the integration numerically performed for 1001 input states with θ' being uniformly distributed over $[0, 2\pi]$. In Fig. 2(d), we have plotted the gate fidelities, where we find that the gate fidelities are $F_N^G = 99.75\%$ and $F_H^G = 99.62\%$.

2.3 Optimal control

Due to the parametric constrain, the previous NHQC implementations are sensitive to the systematic error [52, 53]. Meanwhile, it is difficult to incorporate optimal control technique without additional adjustable parameters. Here, as our scheme introduce additional time dependent phase factors, we can adopt 'zero systematic-error sensitivity'-optimal protocol [56] to further suppress the sensitive of our implementation to the systematic error. To begin with, we consider the static systematic error situation, i.e. $\Omega \rightarrow (1 + \epsilon)\Omega$. Therefore, the Hamiltonian can be written as

$$H_\epsilon(t) = (1 + \epsilon)\Omega e^{i\phi_1} |b\rangle\langle e| + \text{H.c.}, \quad (11)$$

In our implementation, at the end of the first interval $\tau/2$, to evaluate the influence of the static systematic error, the excitation profile is given as

$$P = |\langle \Psi(\tau/2) | \Psi_\epsilon(\tau/2) \rangle|^2 = 1 + \tilde{O}_1 + \tilde{O}_2 + \dots, \quad (12)$$

where $|\Psi_\epsilon(\tau/2)\rangle$ is the state with the static systematic error, and \tilde{O}_m is the perturbation term of order m . Here, we only consider the excitation profile P to the second order, i.e., $P_2 = 1 - \epsilon^2 q_s$, where

$$q_s = -\frac{\partial P_2}{\partial(\epsilon^2)} = \left| \int_0^{\frac{\tau}{2}} e^{-if} \dot{\chi} \sin^2 \chi dt \right|^2 \quad (13)$$

represents the systematic error sensitivity. To nullify the q_s , we set $f(\chi) = n[2\chi - \sin(2\chi)]$, $\varphi_1(0) = 0$ and $\varphi_2(\tau/2) = -\gamma$, which lead to $q_s = \sin^2 n\pi/(2n)^2$, i.e., for positive integer n , $q_s = 0$. When $n \rightarrow 0$, $q_s \rightarrow \pi^2/4$, the current implementation reduces to the previous NHQC case. In the

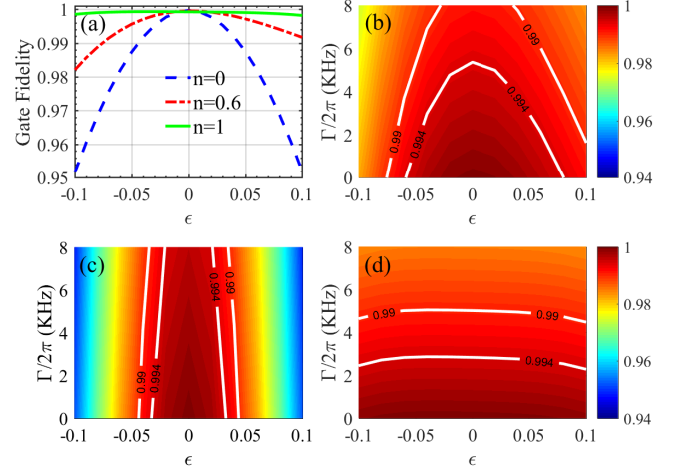


Figure 3 Single-qubit gate performance with optimization. (a) The gate fidelity dynamics of the NOT gate with different values n under the systematic error ϵ without decoherence. (b), (c), and (d) respectively exhibit the gate fidelity dynamics of the NOT gate with optimal value of $n=0.6$, previous NHQC scheme of $n=0$ and $q_s = 0$ case of $n=1$ considering both the systematic error ϵ and decoherence Γ .

following numerical simulations, all the maximum value of Ω are set to be $\Omega_{max} = 2\pi \times 16$ MHz as a restriction. That is the maximum value of the optimized pulse is bounded by Ω_{max} , and thus the improvement of the gate performance can only be attributed to the optimal control.

However, in the case of $n \geq 1$, under the restriction, the evolution time τ will be too long, and decoherence will introduce unacceptable gate infidelity. Therefore, we need to confirm the optimal value of n under the targets with both short time τ and low systematic error sensitivity. To find out the optimal value n under decoherence, we simulated the NOT gate fidelity under the systematic error $-0.1 \leq \epsilon \leq 0.1$ while changing n from 0 to 1 with the uniform step $dn = 0.1$. In this way, we find out that $n = 0.6$ is an optimal value. In Fig. 3(a), we plot the gate fidelity in the case $n = 1$, $n = 0.6$, $n = 0$ without decoherence, respectively. From the Fig. 3(a), we find out that the robustness of the holonomic quantum gates in our scheme is significant improved comparing $n = 1$ with $n = 0$, corresponding to the previous NHQC scheme. From Fig. 3(b), (c) and (d), considering both the systematic error and the decoherence effect, we find that optimal value of $n = 0.6$ is better. Furthermore, for the long coherence time quantum systems, as shown in Fig. 3(d), our scheme will significantly improve the robustness of the holonomic quantum gates.

3 Nontrivial two-qubit gates

In this section, we proceed to implement nontrivial two-qubit quantum gates. Based on the current experimental technique, the strong capacity coupling between transmon qubits has been achieved experimentally on superconducting circuits [60–63]. Here, we consider the case that two transmon qubits are capacitively coupled simultaneously to an auxiliary transmon by the capacity coupling. As shown in Fig. 1(c), the auxiliary transmon with frequency ω_A dispersively coupled to both qubits with frequencies ω_{ge}^k ($k = 1, 2$). Meanwhile, the sequential transitions of both qubits are driven by microwave field with time dependent driving amplitude $\tilde{\Omega}_k(t)$, frequency $\tilde{\omega}_k(t)$ and phase $\tilde{\phi}_k(t)$, i.e. $F_k = \tilde{\Omega}_k(t) \cos[\tilde{\omega}_k(t) + \tilde{\phi}_k(t)]$. In the rotating framework with respect to the driving frequency, the Hamiltonian of the k th qubit coupled to the auxiliary transmon can be written as

$$H_0 = \delta_k N_k - \frac{\alpha_k}{2} (N_k - 1) N_k + \delta_A N_A - \frac{\alpha_A}{2} (N_A - 1) N_A,$$

$$H' = g_k a b_k^\dagger + \frac{\tilde{\Omega}_k e^{i\tilde{\phi}_k}}{2} b_k + \text{H.c.}, \quad (14)$$

where H_0 is the free term of the Hamiltonian for the coupled system, the first two terms represent the nonlinear energy levels of the k th qubit with anharmonicity α_k , and the last two terms represent the nonlinear energy levels of the auxiliary transmon with anharmonicity α_A , and $\delta_k = \omega_{ge}^k - \tilde{\omega}_k$, $\delta_A = \omega_A - \tilde{\omega}_k$, $N_A = a^\dagger a$, $N_k = b_k^\dagger b_k$, with $a = |g\rangle_A \langle e| + \sqrt{2}|e\rangle_A \langle f| + \sqrt{3}|f\rangle_A \langle h| + \dots$, $b_k = |g\rangle_k \langle e| + \sqrt{2}|e\rangle_k \langle f| + \sqrt{3}|f\rangle_k \langle h| + \dots$ being the lower operator for the auxiliary transmon and the qubits. H' is the linear interaction term of the system with the coupling strength g_k between the k th qubit and the auxiliary transmon. As all the sequential transitions are allowed in both qubits, the effective interaction will be generated from the interference of the two paths. In addition, the two couplings form a two-photon resonant situation, i.e., $\omega_{ge}^k - \omega_A = \tilde{\omega}_k - \omega_{ef}^k = \Delta > \alpha_k$, and thus lead to driving-assisted coherent resonant coupling between the auxiliary transmon and the $|g\rangle_k \leftrightarrow |f\rangle_k$ transition of the qubits (see Appendix A for details), the Hamiltonian may be expressed as

$$\tilde{H}_2 = \eta_{ge} |g, e\rangle_{k,A} \langle g, e| + \eta_{fg} |f, g\rangle_{k,A} \langle f, g|$$

$$+ \left(\tilde{g}_k e^{-i\tilde{\phi}_k} |f, g\rangle_{k,A} \langle g, e| + \text{H.c.} \right), \quad (15)$$

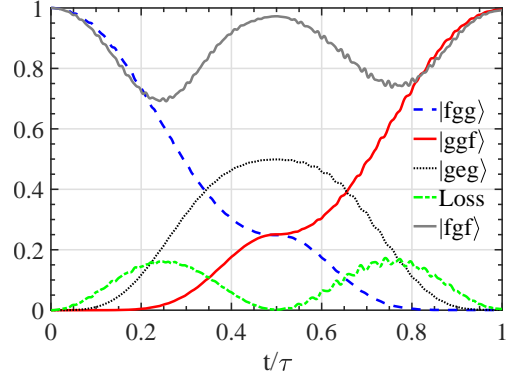


Figure 4 Two-qubit gate performance. State population and fidelity dynamics for gate as a function of time with the initial state being $|fgg\rangle$ with Loss and initial state being $|fgf\rangle$.

where

$$\eta_{ge} = \frac{\tilde{\Omega}_k^2}{4(\Delta - \alpha_k)} - \frac{g_k^2}{\Delta},$$

$$\eta_{fg} = \frac{3\tilde{\Omega}_k^2}{4(\Delta + \alpha_k)} + \frac{2g_k^2}{\Delta - \alpha_k} - \frac{\tilde{\Omega}_k^2}{2\Delta}, \quad (16)$$

$$\tilde{g}_k = \frac{\sqrt{2}g_k\tilde{\Omega}_k}{2(\Delta - \alpha_k)} - \frac{\sqrt{2}g_k\tilde{\Omega}_k}{2\Delta} = \frac{g_k\tilde{\Omega}_k\alpha_k}{\sqrt{2}\Delta(\Delta - \alpha_k)},$$

where the effective resonant interaction strength \tilde{g}_k is induced by the interference of two Raman-like paths, as shown in Fig. 1(c), similar to Ref. [58], and itself and the phase $\tilde{\phi}_k$ can be tunable via tuning the amplitude and phase of the driving field F_k , respectively. Therefore, they can be fine-tuned to meet the requirement for implementing the optimal control in the case of the two-qubits gates.

We set $\Delta \gg \{g_k, \tilde{\Omega}_k\}$, after concealing the cross-Stark-shifts by modulating the frequencies of the driving fields accordingly to $\tilde{\Omega}_k$ (see Appendix B for details), in the single-excitation subspace $S_1 = \text{span}\{|ggf\rangle, |fgg\rangle, |geg\rangle\}$, where $|lms\rangle \equiv |l\rangle_1 \otimes |m\rangle_A \otimes |s\rangle_2$ labels the product states of the two qubits and the auxiliary transmon, the effective interaction Hamiltonian can be described by

$$H_{eff} = \tilde{g}_1 e^{-i\tilde{\phi}_1} |fgg\rangle \langle geg| + \tilde{g}_2 e^{-i\tilde{\phi}_2} |ggf\rangle \langle geg| + \text{H.c.}$$

$$= \tilde{g} e^{-i\tilde{\phi}} |B\rangle \langle E| + \text{H.c.}, \quad (17)$$

where $\tilde{g} = \sqrt{\tilde{g}_1^2 + \tilde{g}_2^2}$, bright state $|B\rangle = \sin(\vartheta/2)|fgg\rangle - e^{-i\tilde{\phi}} \cos(\vartheta/2)|ggf\rangle$ with $\tan(\vartheta/2) = \tilde{g}_1/\tilde{g}_2$ and $\tilde{\phi} = \tilde{\phi}_2 - \tilde{\phi}_1 + \pi$, $|E\rangle = |geg\rangle$, and dark state $|D\rangle = -\cos(\vartheta/2)e^{i\tilde{\phi}}|fgg\rangle - \sin(\vartheta/2)|ggf\rangle$ is decoupled. The above effective Hamiltonian, which can readily be used to implement nontrivial two-qubit gates, establishes a equivalent three-level

Hamiltonian in the single-excitation subspace with $|E\rangle$ being an auxiliary state, as illustrated in Fig. 1(d). Then, we can adopt the same protocol as for the single-qubits case to implement holonomic two-qubit gates. Notably, \tilde{g} and $\tilde{\phi}_1$ in the effective Hamiltonian in Eq. (17) can also be solved by Eq. (2) similar to the single-qubits case, i.e.

$$\tilde{\phi}_1 = \varphi' - \arctan\left(\frac{\chi'}{\phi'} \cot \chi'\right), \tilde{g} = \frac{\chi'}{2 \sin(\tilde{\phi}_1 - \varphi')}, \quad (18)$$

where χ' and φ' are chosen the same form in Eq. (7) and Eq. (8), after that, the effective Hamiltonian can be fixed. Thus, for the case of $\tilde{\gamma} = \pi, \tilde{\phi} = 0$, the evolution operator in the two-qubit gate Hilbert space $S_2 = \text{span}\{|gg\rangle, |gf\rangle, |fg\rangle, |ff\rangle\}$ can be written as

$$U_2(\vartheta) = \begin{pmatrix} 1 & 0 & 0 & 0 \\ 0 & \cos \vartheta & \sin \vartheta & 0 \\ 0 & \sin \vartheta & -\cos \vartheta & 0 \\ 0 & 0 & 0 & 1 \end{pmatrix}. \quad (19)$$

Now, we analyse the performance of two-qubit gates with $\vartheta = \pi/2$. For $\Delta = 2\pi \times 1$ GHz, and the parameter of transmons $g_k = 2\pi \times 65$ MHz, $\alpha_k = 2\pi \times 400$ MHz, $\alpha_A = 2\pi \times 370$ MHz, $\tau_2 = 57$ ns, $\tilde{g}_{k,max} = 10$ MHz by modulating $\tilde{\Omega}_k(t)$ with the maximum value to be $2\pi \times 320$ MHz. When the initial state is $|fgg\rangle$, a fidelity of 99.44% can be obtained, as plotted in Fig. 4, which is done by using the origin Hamiltonian in Eq.(14), i.e., including all the unwanted higher-order effects induced by the strong microwave driving. In addition, the loss represents the leakage from our computational basis to neighboring states caused directly by the time dependence of the amplitude of the driving pulse, leading to the time dependence of the cross-ac-Stark-shifts terms, which can be compensated by modulating the pulse frequencies $\tilde{\omega}_k$ accordingly. Notably, due to the amplitude of the driving pulse being zero at the beginning and the ending of the evolution, as we conceal the cross-ac-Stark-shifts, the loss is zero before and after the operation. Similarly, the optimal control technique presented in the single-qubit implementation can also be incorporated in this two-qubit gate implementation.

4 Discussion and conclusion

In conclusion, we have proposed a practical implementation of fast NHQC on capacitively coupled superconducting circuits with microwave fields induced effective resonant coupling. Our scheme can be scaled up to two-dimensional square lattice of qubits, which is a scalable setup for QC. Besides the scalability, our scheme has the

following additional distinct merits. First, instead of linear resonators, auxiliary transmons are used to induced nontrivial two-qubit gates, the intrinsic nonlinearity of which can be large enough for our purpose. On the other hand, using the transmons to serve as auxiliary elements makes our scalable setup consists only the qubits, and thus easier to be fabricated. Second, due to the fine inverse Hamiltonian engineering, the evolution state of our proposal has two independent variables, thus it meets the minimal requirement of optimal control techniques, which can be used to further enhances the robustness of our implementation. Therefore, our scheme removes the main obstacles of NHQC, and thus provides a promising way towards robust NHQC on superconducting circuits.

Appendix

A The effective Hamiltonian

Starting from the original Hamiltonian of Eq. (14) in the main text, the energies of the state $|g, e\rangle, |f, g\rangle$ are

$$E_{f,g} = 2\delta_k - \alpha_k, \quad E_{g,e} = \delta_A, \quad (20)$$

which can be adjusted to be degenerate by modulating $\tilde{\omega}_k$ such that $\delta_A = 2\delta_k - \alpha_k$, and set $\varepsilon = E_{f,g} = E_{g,e}$. We then define

$$\mathcal{P} = |g, e\rangle_{k,A} \langle g, e| + |f, g\rangle_{k,A} \langle f, g|, \quad (21)$$

$$\mathcal{X} = \sum_{\Pi} \frac{|l, m\rangle_{k,A} \langle l, m|}{\varepsilon_{l,m} - \varepsilon}, \quad (22)$$

where the degenerate subspace $\{|g, e\rangle_{k,A}, |f, g\rangle_{k,A}\}$ is of interest, $\Pi : \{l, m | (l, m) \neq (g, e) \text{ or } (f, g)\}$, and $\varepsilon_{l,m}$ is the energy of state $|l, m\rangle$. In the following, we only consider the fourth energy level that is beyond the qubit states.

We handle the effective Hamiltonian using a perturbation theory with $\{g_k, \tilde{\Omega}_k\} \ll \Delta = \delta_k - \delta_A$, the first-order term is found to be

$$\tilde{H}_1 = \mathcal{P} H' \mathcal{P} = 0, \quad (23)$$

as

$$\begin{aligned} H' \mathcal{P} = & \left(g_k |e, g\rangle + \frac{\tilde{\Omega}_k}{2} e^{-i\tilde{\phi}_k} |e, e\rangle \right)_{k,A} \langle g, e| \\ & + \left(\sqrt{2} g_k |e, e\rangle + \frac{\sqrt{2}\tilde{\Omega}_k}{2} e^{i\tilde{\phi}_k} |e, g\rangle \right. \\ & \left. + \frac{\sqrt{3}\tilde{\Omega}_k e^{-i\tilde{\phi}_k}}{2} |h, g\rangle \right)_{k,A} \langle f, g|. \end{aligned} \quad (24)$$

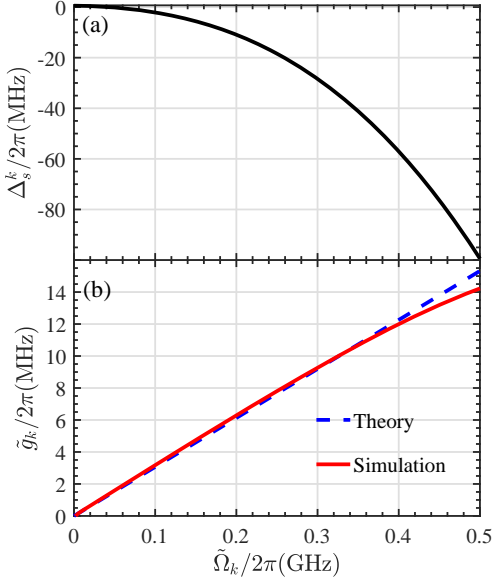


Figure 5 (a) Illustration of the Δ_s^k with respect to $\tilde{\Omega}_k$ for fixed g_k . (b) Illustration of the effective transmon-transmon coupling strength \tilde{g} with respect to $\tilde{\Omega}_k$ with fixed g_k .

As for the second-order terms,

$$\begin{aligned} \tilde{H}_2 &= -\mathcal{P} H' \mathcal{K} H' \mathcal{P} \\ &= -\mathcal{P} H' (\mathcal{K}_1 + \mathcal{K}_2 + \mathcal{K}_3) H' \mathcal{P}, \end{aligned} \quad (25)$$

where

$$\begin{aligned} \mathcal{K}_1 &= \frac{|e, g\rangle_{k,A} \langle e, g|}{\varepsilon_{e,g} - \varepsilon}, \\ \mathcal{K}_2 &= \frac{|e, e\rangle_{k,A} \langle e, e|}{\varepsilon_{e,e} - \varepsilon}, \\ \mathcal{K}_3 &= \frac{|h, g\rangle_{k,A} \langle h, g|}{\varepsilon_{h,g} - \varepsilon}. \end{aligned}$$

Finally, we get the Eq.(15) in main text.

B Compensate of the cross-ac-Stark-shifts

In Eq. (15), there are just ac Stark shifts caused by the k th qubit coupled to an auxiliary transmon. When we consider the two qubits simultaneously coupled to an auxiliary transmon, the cross-ac-Stark-shifts will occur [44]. In the degenerate subspace S_1 , the whole Hamiltonian can

be written as

$$\begin{aligned} H_{\text{two}} &= \eta_{fgg} |f g g\rangle \langle f g g| + \eta_{geg} |g e g\rangle \langle g e g| \\ &\quad + \eta_{ggf} |g g f\rangle \langle g g f| + \tilde{g}_1 e^{-i\tilde{\phi}_1} |f g g\rangle \langle g e g| \\ &\quad + \left(\tilde{g}_2 e^{-i\tilde{\phi}_2} |g g f\rangle \langle g e g| + \text{H.c.} \right) \\ &= \eta_B |B\rangle \langle B| + \eta_D |D\rangle \langle D| + \eta_E |E\rangle \langle E| \\ &\quad + \left(\tilde{g} e^{-i\tilde{\phi}_1} |B\rangle \langle E| + \text{H.c.} \right), \end{aligned} \quad (26)$$

where η_M is the energy level shift of the state $|M\rangle$. Due to the existence of the cross-ac-Stark-shifts, it can lead to large errors of the gate operations. Therefore, we need to compensate these shifts. It is noted that both g_k and $\tilde{\Omega}_k$ split the degenerate subspace $\{|B\rangle, |D\rangle, |E\rangle\}$, so we will fix g_k and tune the frequency $\tilde{\omega}_k$ of the driven field to fulfill $|\eta_B - \eta_E| = |\eta_B - \eta_D| = 0$. However, as $|\eta_B - \eta_E| \geq |\eta_B - \eta_D|$ due to \tilde{g} , we just need to care $|\eta_B - \eta_E| = 0$ in the degenerate subspace $\{|B\rangle, |E\rangle\}$, i.e.,

$$\langle \phi_l(\tilde{\Omega}_k) | \frac{d}{d\tilde{\Omega}_k(t)} | \phi_m(\tilde{\Omega}_k) \rangle = 0.$$

Then, we obtain

$$\begin{aligned} &\langle \phi_l(\tilde{\Omega}_k) | \frac{\partial H}{\partial \tilde{\Omega}_k} | \phi_m(\tilde{\Omega}_k) \rangle \\ &+ \frac{d\tilde{\omega}_k}{d\tilde{\Omega}_k} \langle \phi_l(\tilde{\Omega}_k) | \frac{\partial H}{\partial \tilde{\Omega}_k} | \phi_m(\tilde{\Omega}_k) \rangle = 0, \end{aligned} \quad (27)$$

which can be numerically solved to obtain the $\tilde{\omega}_k - \tilde{\Omega}_k$ curve, such that one can figure out the $\Delta_s^k = \tilde{\omega}_k - \tilde{\omega}_k(0)$ under the situation $\tilde{\Omega}_1 = \tilde{\Omega}_2$ for numerical simulation, as shown in Fig. 5(a). Once the above equation is satisfied, the cross-ac-Stark-shifts must be compensated by tuning the frequency $\tilde{\omega}_k$ of the driven field.

After that, in order to effectively conceal the cross-ac-Stark-shifts, the driven pulse with smoothly changed amplitude can be employed, which can lead to a smoothly changed effectively resonant coupling strength \tilde{g}_k . As shown in Fig. 5(b), the $\tilde{g}_k - \tilde{\Omega}_k$ curve of the numerical simulation is coincident to the theory. Also note that when $\tilde{\Omega}_k$ is large, the trend of $\tilde{g}_k - \tilde{\Omega}_k$ will be slightly nonlinear.

Acknowledgments

This work was supported by the Key-Area Research and Development Program of Guangdong Province (Grant No. 2018B030326001), the National Natural Science Foundation of China (Grant No. 11874156), the National Key R&D Program of China (Grant No. 2016 YFA0301803), and the research project from SCNU (Grant No. 19WDGB04).

Conflict of Interest

The authors declare no conflict of interest.

Key words. Geometric quantum computation, superconducting circuits, optimal control

References

- [1] M. V. Berry, *Proc. R. Soc. Lond., Ser. A* **1984**, 392, 45.
- [2] F. Wilczek, A. Zee, *Phys. Rev. Lett.* **1984**, 52, 2111.
- [3] Y. Aharonov, J. Anandan, *Phys. Rev. Lett.* **1987**, 58, 1593.
- [4] P. Solinas, P. Zanardi, N. Zanghì, *Phys. Rev. A* **2004**, 70, 042316.
- [5] S. L. Zhu, P. Zanardi, *Phys. Rev. A* **2005**, 72, 020301(R).
- [6] P. Solinas, M. Sassetti, T. Truini, N. Zanghì, *New J. Phys.* **2012**, 14, 093006.
- [7] M. Johansson, E. Sjöqvist, L. M. Andersson, M. Ericsson, B. Hessmo, K. Singh, D. M. Tong, *Phys. Rev. A* **2012**, 86, 062322.
- [8] E. Sjöqvist, *Physics* **2008**, 1, 35.
- [9] P. Zanardi, M. Rasetti, *Phys. Lett. A* **1999**, 264, 94.
- [10] X. B. Wang, M. Keiji, *Phys. Rev. Lett.* **2001**, 87, 097901.
- [11] S. L. Zhu, Z. D. Wang, *Phys. Rev. Lett.* **2002**, 89, 097902.
- [12] E. Sjöqvist, D. M. Tong, L. M. Andersson, B. Hessmo, M. Johansson, K. Singh, *New J. Phys.* **2012**, 14, 103035.
- [13] G. F. Xu, J. Zhang, D. M. Tong, E. Sjöqvist, L. C. Kwek, *Phys. Rev. Lett.* **2012**, 109, 170501.
- [14] V. A. Mousolou, E. Sjöqvist, *Phys. Rev. A* **2014**, 89, 022117.
- [15] J. Zhang, L. C. Kwek, E. Sjöqvist, D. M. Tong, P. Zanardi, *Phys. Rev. A* **2014**, 89, 042302.
- [16] G. F. Xu, G. L. Long, *Sci. Rep.* **2014**, 4, 6814.
- [17] G. F. Xu, C. L. Liu, P. Z. Zhao, D. M. Tong, *Phys. Rev. A* **2015**, 92, 052302.
- [18] Z. Y. Xue, J. Zhou, Z. D. Wang, *Phys. Rev. A* **2015**, 92, 022320.
- [19] E. Sjöqvist, *Phys. Lett. A* **2016**, 380, 65.
- [20] Z. Y. Xue, J. Zhou, Y. M. Chu, Y. Hu, *Phys. Rev. A* **2016**, 94, 022331.
- [21] P. Z. Zhao, G. F. Xu, D. M. Tong, *Phys. Rev. A* **2016**, 94, 062327.
- [22] E. Herterich, E. Sjöqvist, *Phys. Rev. A* **2016**, 94, 052310.
- [23] G. F. Xu, P. Z. Zhao, T. H. Xing, E. Sjöqvist, D. M. Tong, *Phys. Rev. A* **2017**, 95, 032311.
- [24] Z. Y. Xue, F. L. Gu, Z. P. Hong, Z. H. Yang, D. W. Zhang, Y. Hu, J. Q. You, *Phys. Rev. Appl.* **2017**, 7, 054022.
- [25] G. F. Xu, P. Z. Zhao, D. M. Tong, E. Sjöqvist, *Phys. Rev. A* **2017**, 95, 052349.
- [26] P. Z. Zhao, G. F. Xu, Q. M. Ding, E. Sjöqvist, D. M. Tong, *Phys. Rev. A* **2017**, 95, 062310.
- [27] V. A. Mousolou, *Phys. Rev. A* **2017**, 96, 012307.
- [28] J. Zhou, B. J. Liu, Z. P. Hong, Z. Y. Xue, *Sci. China: Phys. Mech. Astron.* **2018**, 61, 010312.
- [29] Z. P. Hong, B. J. Liu, J. Q. Cai, X. D. Zhang, Y. Hu, Z. D. Wang, Z. Y. Xue, *Phys. Rev. A* **2018**, 97, 022332.
- [30] G. F. Xu, D. M. Tong, E. Sjöqvist, *Phys. Rev. A* **2018**, 98, 052315.
- [31] V. A. Mousolou, *Phys. Rev. A* **2018**, 98, 062340.
- [32] F. Zhang, J. Zhang, P. Gao, G. Long, *Phys. Rev. A* **2019**, 100, 012329.
- [33] N. Ramberg, E. Sjöqvist, *Phys. Rev. Lett.* **2019**, 122, 140501.
- [34] A. A. Abdumalikov, J. M. Fink, K. Juliusson, M. Pechal, S. Berger, A. Wallraff, S. Filipp, *Nature (London)* **2013**, 496, 482.
- [35] G. Feng, G. Xu, G. Long, *Phys. Rev. Lett.* **2013**, 110, 190501.
- [36] C. Zu, W. B. Wang, L. He, W. G. Zhang, C. Y. Dai, F. Wang, L. M. Duan, *Nature (London)* **2014**, 514, 72.
- [37] S. Arroyo-Camejo, A. Lazariev, S. W. Hell, G. Balasubramanian, *Nat. Commun.* **2014**, 5, 4870.
- [38] Y. Sekiguchi, N. Niikura, R. Kuroiwa, H. Kano, H. Kosaka, *Nat. Photonics* **2017**, 11, 309.
- [39] B. B. Zhou, P. C. Jerger, V. O. Shkolnikov, F. J. Heremans, G. Burkard, D. D. Awschalom, *Phys. Rev. Lett.* **2017**, 119, 140503.
- [40] H. Li, L. Yang, G. Long, *Sci. China: Phys., Mech. Astron.* **2017**, 60, 080311.
- [41] Y. Xu, W. Cai, Y. Ma, X. Mu, L. Hu, T. Chen, H. Wang, Y. P. Song, Z. Y. Xue, Z. Q. Yin, L. Sun, *Phys. Rev. Lett.* **2018**, 121, 110501.
- [42] N. Ishida, T. Nakamura, T. Tanaka, S. Mishima, H. Kano, R. Kuroiwa, Y. Sekiguchi, H. Kosaka, *Opt. Lett.* **2018**, 43, 2380.
- [43] K. Nagata, K. Kuramitani, Y. Sekiguchi, H. Kosaka, *Nat. Commun.* **2018**, 9, 3227.
- [44] D. J. Egger, M. Ganzhorn, G. Salis, A. Fuhrer, P. Muller, P. K. Barkoutsos, N. Moll, I. Tavernelli, S. Filipp, *Phys. Rev. Appl.* **2019**, 11, 014017.
- [45] T. Yan, B. J. Liu, K. Xu, C. Song, S. Liu, Z. Zhang, H. Deng, Z. Yan, H. Rong, K. Huang, M. H. Yung, Y. Chen, D. Yu, *Phys. Rev. Lett.* **2019**, 122, 080501.
- [46] Z. Zhu, T. Chen, X. Yang, J. Bian, Z. Y. Xue, X. Peng, *Phys. Rev. Appl.* **2019**, 12, 024024.
- [47] J. Clarke, F. K. Wilhelm, *Nature (London)* **2008**, 453, 1031.
- [48] J. Q. You, F. Nori, *Nature (London)* **2011**, 474, 589.
- [49] M. H. Devoret, R. J. Schoelkopf, *Science* **2013**, 339, 1169.
- [50] J. Koch, T. M. Yu, J. Gambetta, A. A. Houck, D. I. Schuster, J. Majer, A. Blais, M. H. Devoret, S. M. Girvin, R. J. Schoelkopf, *Phys. Rev. A* **2007**, 76, 042319.
- [51] M. J. Peterer, S. J. Bader, X. Jin, F. Yan, A. Kamal, T. J. Gudmundsen, P. J. Leek, T. P. Orlando, W. D. Oliver, S. Gustavsson, *Phys. Rev. Lett.* **2015**, 114, 010501.
- [52] S. B. Zheng, C. P. Yang, F. Nori, *Phys. Rev. A* **2016**, 93, 032313.
- [53] J. Jing, C. H. Lam, L. A. Wu, *Phys. Rev. A* **2017**, 95, 012334.

- [54] B. J. Liu, X. K. Song, Z. Y. Xue, X. Wang, M. H. Yung, *Phys. Rev. Lett.* **2019**, *123*, 100501.
- [55] D. Daems, A. Ruschhaupt, D. Sugny, S. Guérin, *Phys. Rev. Lett.* **2013**, *111*, 050404.
- [56] A. Ruschhaupt, X. Chen, D. Alonso, J. G. Muga, *New J. Phys.* **2012**, *14*, 093040.
- [57] R. Barends, J. Kelly, A. Megrant, A. Veitia, D. Sank, E. Jeffrey, T. C. White, J. Mutus, A. G. Fowler, B. Campbell, Y. Chen, Z. Chen, B. Chiaro, A. Dunsworth, C. Neill, P. OařMalley, P. Roushan, A. Vainsencher, J. Wenner, A. N. Korotkov, A. N. Cleland, J. M. Martinis, *Nature (London)* **2014**, *508*, 500.
- [58] S. Zeytinođlu, M. Pechal, S. Berger, A. A. Abdumalikov Jr., A. Wallraff, S. Filipp, *Phys. Rev. A* **2015**, *91*, 043846.
- [59] J. F. Poyatos, J. I. Cirac, P. Zoller, *Phys. Rev. Lett.* **1997**, *78*, 390.
- [60] M. H. Goerz, F. Motzoi, K. B. Whaley, C. P. Koch, *npj Quantum Inf.* **2017**, *3*, 37.
- [61] M. Reagor *et al.*, *Sci. Adv.* **2018**, *4*, eaao3603.
- [62] S. A. Caldwell *et al.*, *Phys. Rev. Appl.* **2018**, *10*, 034050.
- [63] X. Li, Y. Ma, J. Han, T. Chen, Y. Xu, W. Cai, H. Wang, Y. P. Song, Z. Y. Xue, Z. Q. Yin, L. Sun, *Phys. Rev. Appl.* **2018**, *10*, 054009.